References

[1] M.A. Sainz, A. Duran, J.M. Fernandez Navarro, J. Non-Cryst. Solids 121 (1990) 315.
[2] M.S. Al- Robaee, K.N. Rao, S. Mohan, J. Appl. Phys. 71 (1992) 2380.
[3] S.Y. Zheng, A.M. Andersson-Faldt, B. Stjerna, C.G. Granqvist, Appl. Opt. 32 (1993) 6303.
[4] M. Ghanashyam Krishna, A. Hartridge, A.K. Bhattaharya, Mater. Sci. Eng. B55 (1998) 14.
[5] T. Inoue, M. Osonoe, H. Tohda, M. Hiramatsu, J. Appl. Phys. 69 (1991) 8313.
[6] B.E. Park, I. Sakai, E. Sakai, E. Tokumitsu, H. Ishiwara, Appl. Surf. Sci. 117/118 (1997) 423.
[7] R.M. Bueno, J.M. Martinez-Duart, M. Hernandez-Velez, L. Vazquez, J. Mater. Sci. Eng. 32 (1997) 1861.
[8] M. Stromme Mattson, A. Azens, G.A. Niklasson, C.G. Granqvist, J. Purans, J. Appl. Phys. 81 (1997) 6432.
[9] S. Kanakaraju, S. Mohan, A.K. Sood, Thin Solid Films 305 (1997) 191.
[10] T. Ami, M. Suzuki, Mater. Sci. Eng. B54 (1998) 84.
[11] K. Jarrendahl, H. Arwin, Thin Solid Films 313 (1998) 114.
[12] F. Varsano, F. Decker, E. Massetti, F. Cardellini, A. Licciuli, Electrochim. Acta 44 (1999) 103.
[13] T. Morishiata, Chem. Vap. Dep. 2 (1996) 191.
[14] W.B. Carter, G.W. Book, T.A. Polley, D.W. Stollberg, J.M. Hampikian, Thin Solid films 347 (1999) 25.
[15] C. Tian, Y. Du, S.W. Chan, Mater. Res. Soc. Proc V. 355 (1995) 513.
[16] K.D. Develos, M. Kusunoki, S. Ohshima, Jpn. J. Appl. Phys. 37 (1998) 6161.
[17] P. Baudry, A.C.M. Rodrigues, M. Aegerter, L.O. Bulhoes, Mater. J. Non Crys. Solids 121 (1990) 319.
[18] D. Keomany, J.P. Pettit, D. Deroo, SPIE Proc. V. 2255 (1995) 513.
[19] M.A. Aegerter, in: R. Reisfeld, C.K. Jorgensen (Eds.), Sol–Gel Chromogenic Materials and Devices, Vol. 85. Structure and Bonding, Springer, Berlin, 1996, pp. 149–194.
[20] N. Ozer, J.P. Cronin, S. Akyuz, Proc. SPIE V. 3788 (1999) 103.
[21] C.J. Brinker, G.W. Scherer, Sol–Gel Science, Academic Press, New York, 1990, pp.180-189.
[22] C.G. Granqvist, Handbook of Inorganic Electrochromic Materials, Elsevier, Amsterdam, The Netherlands, 1995.
[23] A. Azens, L. Kullman, Solar Energy. Mater. Solar. Cells 56 (1999) 193.
[24] J. Tonazzi, B. Valla, M.A. Macedo, P. Baudry, M.A. Aegerter, Proc. SPIE V. 1328 (1990) 375.
[25] D.P. Arndt et al., Appl. Opt. 23 (1984) 3571.
[26] C.D. Wagner, W.M. Riggs, L.E. Davis, J.F. Moulder, G.E. Mullenberg, Handbook of X-ray Photoelectron Spectroscopy, Perkin Elmer Corp, Eden Prairie, Minnesota, USA, 1990.
[27] J. Tauc, R. Grigorovici, A. Vancu, Phys. Stat. Solidi 15 (1996) 455.
[28] F. Wooten, Optical properties of Solids, Academic Press, New York, USA, 1981.
[29] D. Keomany, C. Poinsignon, D. Deroo, Solar Energy Mater. Solar Cells 36 (1995) 397.

Sol–gel niobium pentoxide: A promising material for electrochromic coatings, batteries, nanocrystalline solar cells and catalysis

Michel A. Aegerter*

Department of Coating Technology, Institut für Neue Materialien, INM, Gebäude 43 D - 66123 Saarbrücken, Germany

Abstract

In the last decade the sol–gel process became a promising method to synthesize materials in form of coatings, nanoscale powders and porous systems. The technique has been mainly used at laboratory scale and has brought interesting contributions for the development of new nanomaterials. Nevertheless, several products or devices made with such a process already exist and new ones should be available in the market in the near future. This paper briefly reviews the state of the art in the development of electrochromic (EC) coatings and devices, batteries, nanocrystalline solar cells and in the field of catalysis achieved during the last decade using sol–gel derived pure and doped *niobium pentoxide*.

Keywords: Sol–gel; Niobium oxide; Coating; Aerogel; Electrochromism; Solar cell; Battery; Catalysis

1. Introduction

Stoichiometric niobium oxides mainly exist in the form of NbO, Nb_2O_3, NbO_2 and α, β Nb_2O_5 [1]. The first two compounds have been obtained by melting the richest niobium oxide, Nb_2O_5, with Nb at high temperature. Non-stoichiometric suboxide phases have also been observed. Niobium pentoxide, also known as niobia or niobic acid anhydride, is however the most studied material. It has been prepared by different methods such as oxidation of metallic niobium in air, by hydrolyzing

*Tel.: + 49-681-9300-317; fax: + 49-681-9300-249.
E-mail address: aegerter@inm-gmbh.de (M.A. Aegerter).

alkali-metal niobates, niobium alkoxides and niobium pentachloride or by precipitation from solution in hydrofluoric acid with alkali-metal hydroxide or ammonia [2]. Nb_2O_5 possesses a quite complex crystalline morphology as at least 12 structures have been identified. The phases most often found have been labeled T, TT, B, M and H [3,4] and their appearance depends on the preparation method of the compound and the kinetics and thermodynamics. Fig. 1 shows an example of the phases obtained as a function of the temperature starting from amorphous niobium oxide. The T and TT phases are essentially observed below 800°C and the TT phase, indexed as pseudohexagonal, is thought to be a modification of the orthorhombic T phase as it presents a lower crystallinity and is probably stabilized by impurities such as OH^-, Cl^- or vacancies [5].

Stoichiometric Nb_2O_5 is an insulator [1] with, for example, a conductivity of $\sigma = 3 \times 10^{-6}$ S/cm for a H-type Nb_2O_5 single crystal. However, it becomes an n-type semiconductor at lower oxygen content and $Nb_2O_{4.978}$ has a conductivity $\sigma = 3 \times 10^3$ S/cm. The conduction band is built from the 3d orbitals of Nb atoms and the valence band from the 2p orbitals of oxygen. The band gap observed from optical measurements varies between 3.2 and 4 eV. The index of refraction n and density ρ both depend on the crystalline phase: for amorphous niobia n was found to vary from 2.0 to 2.26 and ρ from 4.36 to 5.12 g/cm^3. For the TT and T phase ρ takes the values of 4.99 and 5.00 g/cm^3, respectively [1].

Traditionally, niobium pentoxide is used in metallurgy for the production of hard materials or in optics as additive to prevent the devitrification and to control the refractive index of special glasses. In electronics it is used for the preparation of electroacoustic or eletrooptical components such as $LiNbO_3$ and $KNbO_3$ or relaxor ferroelectric ceramics such as $Pb(Mg_{1/3}Nb_{2/3})O_3$ [2]. However, in the last 15 years, its interesting semiconducting properties and the advent of more sophisticated methods of preparation allowed to obtain in a controlled way of innovative systems such as highly porous materials, very fine powders and coatings. These new materials have found further important application in the fields of electrochromism, batteries, solar cells and catalysis.

This paper briefly reviews the recent results obtained for these new applications with pure and doped *niobium pentoxide* prepared by the *sol–gel* process, although some references are also given for comparison and for other preparation routes.

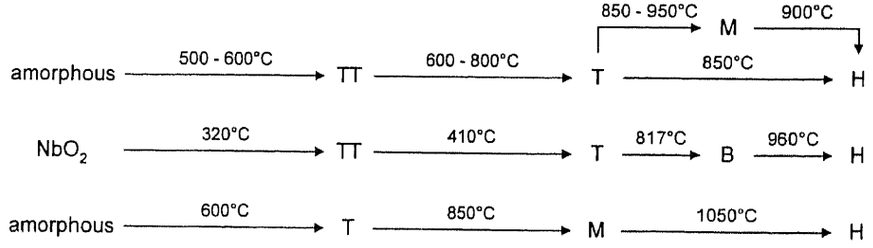

Fig. 1. Temperature evolution of the most important crystalline phases of niobium oxide (amorphous, TT, T, M, and H) for different preparation methods according to Refs. [4] (a, b) and [3] (c).

The *sol–gel* method was recognized as a promising route for the preparation of niobium oxide gels, powders and coatings only in 1986 by Alquier et al. [6] who presented four different routes for the synthesis of sols and gels: the dissolution of $NbCl_5$ in water with or without addition of hydrogen peroxide, the "classical" but expensive way using alkoxides (e.g. $Nb(OEt)_5$) and a cheaper synthesis using chloroalkoxides. Griesmar et al. [7] from the same laboratory later showed the possibility to obtain Nb_2O_5 xerogels by reactively modifying (with acetic acid) $Nb(OPent^n)_5$, previously synthesized by reacting $Nb(OEt)_5$ with n-pentanol. These authors only mentioned that such chemical routes could also be useful to prepare coatings but only amorphous phases (gels) and, upon heating in air at 500°C, pure tetragonal niobium pentoxide powders have been obtained. A characterization concerning the above applications has not been presented. Hence, the use of *sol–gel* derived niobium oxide for electrochromic coatings and devices, solar cells, batteries and catalysis is quite recent.

In the past 10 years, most of the development has been realized in the field of electrochromism (EC) which is reviewed first in Section 2. The results obtained for the realization of batteries, nanocrystalline solar cells (Graetzel cells) and catalysis are then reported in Sections 3, 4 and 5, respectively. A conclusion follows in Section 6.

2. Nb_2O_5 electrochromic (EC) coatings and devices

The first mention of the electrochromic properties of Nb_2O_5 coatings, i.e. a persistent but reversible optical change produced electrochemically, was published by Reichman and Bard in 1980 to our knowledge [8]. Such an effect was observed with a 15 μm thick coating produced on the surface of a niobium metallic disk oxidized at approximately 500°C for 10 min. A blue coloring effect, seen in reflection under H^+ and later also under Li^+ insertion [9], was chemically stable and showed fast kinetics (1–2 s).

Since then several more adequate deposition techniques have been used to obtain niobium oxide EC films among which CVD [10], DC magnetron sputtering [11], electrochemical method [12] and the dip or spin coating process via the *sol–gel* route. More general reviews on the preparation and on the electrochromic properties of coatings and devices prepared by the *sol–gel* method (including Nb_2O_5) have already been given by Agrawal et al. [13] and the author [14–16].

2.1. *Pure niobium oxide sol–gel coatings and devices*

Lee and Crayston [17] were the first to show that pure sol-gel Nb_2O_5 coatings present an electrochromic effect. They prepared 5–10 μm thick coatings by spinning a hydrolyzed solution of $NbCl_5$ dissolved in ethanol on ITO coated glass. Although substantial cracking and peeling effects due to an important shrinkage were observed, the films showed a blue coloration with fast coloration (approx. 6 s) and bleaching (approx. 3 s) kinetics and a coloration efficiency of 6 cm^2/C. However, the durability of the EC response was only a few cycles although the quality of the films could be

improved by adding trialkoxysilane (Glymo®) in the solution. A slightly higher coloration efficiency was then reported by Faria et al. [18] who prepared 2.8 μm thick coatings using a sol made by dissolving citric acid in ethylene glycol to which was added a niobium oxalate complex $NH_4H_2[NbO(C_2O_4)_3] \times 3H_2O$. The films also showed a blue color under Li insertion with a transmission change at 631 nm from 80% to 30%. Much better results have been obtained by Ohtani et al. [19] and Özer et al. [20,21] using sols made from niobium alkoxides such as $Nb(OEt)_5$ and by Aegerter et al. [22–24] who synthesized $Nb(OBu^n)_5$ by reacting $NbCl_5$ with sodium butoxide in butanol, which is now called the Na route [25]. The improvement in the EC properties of the layers was essentially due to the fact that the layers obtained with these precursors were thin (typically 100–150 nm) and consequently of much better quality even if the deposition procedure had to be repeated 2–4 times in order to get a coating presenting larger change in optical transmission under H^+ or Li^+ insertion. Aegerter et al. [26–28] also developed a cheaper sol synthesis by dissolving $NbCl_5$ in butanol and acetic acid under strong ultrasonic irradiation (sonocatalysis). The procedure leads to a niobium chloroalkoxide ($NbCl_{5-x}(OBu)_x$). The method was then extended to other alkoxy groups by Schmitt et al. [29] who dissolved niobium chloride in ethanol and by Macek et al. [30,31] who used a sol made by dissolving $NbCl_5$ in propanol, following a method described by Barros Filho et al. [32]. The last authors succeeded to prepare single (132 nm thick) and multilayers EC films sintered at 500°C which showed a high blue transmission change in the visible from 80% down to 30% by inserting up to 31.6 mC/cm^2 Li^+ ions.

From the above reports it clearly appears that till today the best niobium oxide coatings for EC purpose prepared by the *sol–gel* process are those made from alkoxides- or chloroalkoxides-based sols. The choice of the precursor does not seem to have a large influence on the final EC properties and if devices have to be made, the dissolution of $NbCl_5$ in an alcohol under a sonocatalysis process is surely the fastest and cheapest procedure. However, according to Schmitt et al. [29,33], the amount of lithium ions which can be inserted reversibly into the films as well as the corresponding change of the optical density both decrease with increasing length of the alkyl chain. Therefore, ethanol is the preferred solvent for the sol preparation. Large indium tin oxide (ITO) or fluorine-doped tin oxide (FTO) coated glass substrates can thus be coated by the dip coating process at a withdrawal rate of typically 2 mm/s. Depending on the sol concentration the resulting films are relatively thin (30–140 nm) and the coating procedure has to be repeated several times to obtain thick coatings, each layer being previously dried and partly sintered at 400°C before the next deposition step. Thick coating stacks can be sintered up to 600°C, which is the highest temperature allowed to keep the commercial conductive substrates with good properties.

It is difficult to compare the results of the different working groups as coating thickness, the sintering temperature and the size of the samples are usually different. The combined electrochemical and optical investigations were also realized under different configurations (electrolyte, applied voltage, number of cycles, electrochemical methods, etc.). We give here as an example some results obtained recently by Schmitt et al. [29,33] for pure Nb_2O_5 who summarized the state of the art obtained with this material. The coatings have been deposited by the dip-coating process using

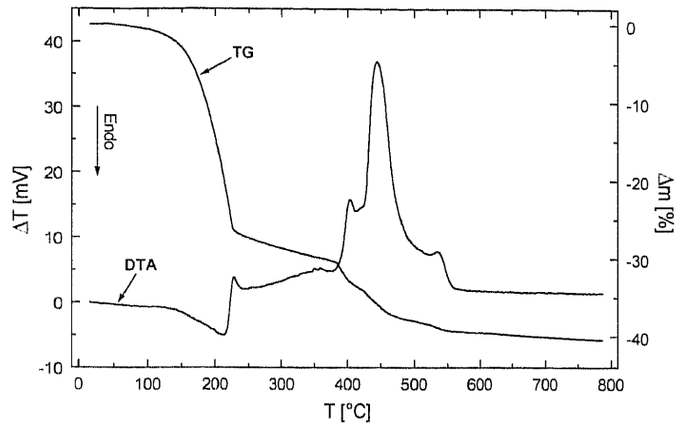

Fig. 2. DTA and TG curves measured at 10 K/min of a Nb_2O_5 xerogel dried at 100°C prepared by the chloroalkoxide route [29,33].

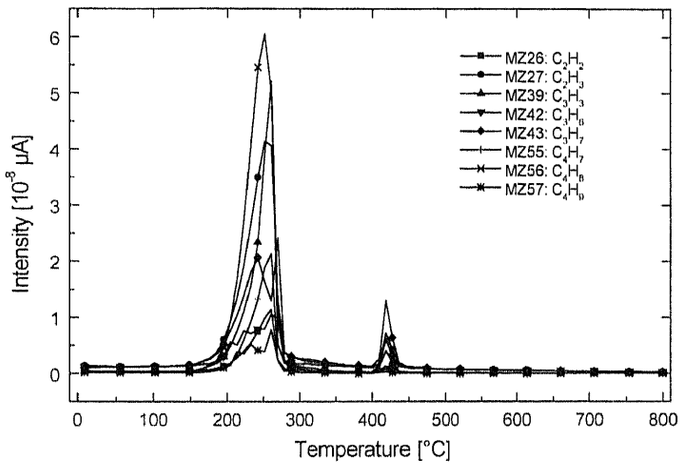

Fig. 3. C_xH_y fractions mass spectrometry analysis of the Nb_2O_5 xerogel of Fig. 2 [29,33].

sols obtained by the chloroalkoxide route, i.e. by dissolving $NbCl_5$ in ethanol and acetic acid [29,33]. Fig. 2 shows a typical differential thermal analysis (DTA) and thermogravimetry (TG) of a pure Nb_2O_5 xerogel dried at 100°C. An endothermic peak is first observed at about 200°C followed by an exothermic peak at 250°C. Both the peaks are accompanied by a 9% mass loss essentially due to the evolution of the solvent molecules (fraction of the type C_xH_y (mass 26, 27, 39, 42, 43, 55, 66, 57) and, to a minor extent, the evolution of HCl (mass 36 and 37)) as confirmed by a simultaneous mass spectrometry (MS) analysis (Figs. 3 and 4). These results are indicative of the

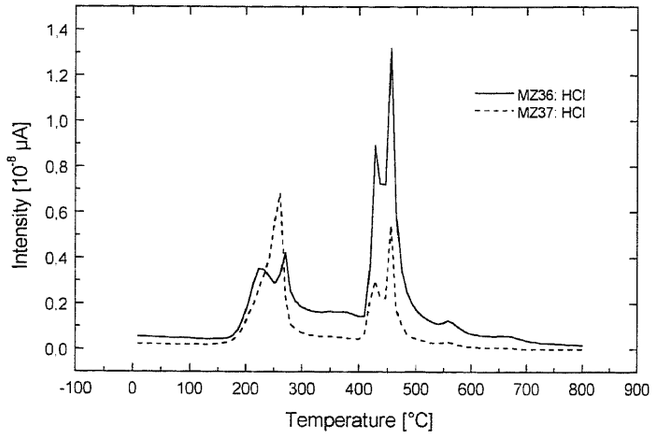

Fig. 4. HCl mass spectrometry analysis of the Nb_2O_5 xerogel of Fig. 2 [29,33].

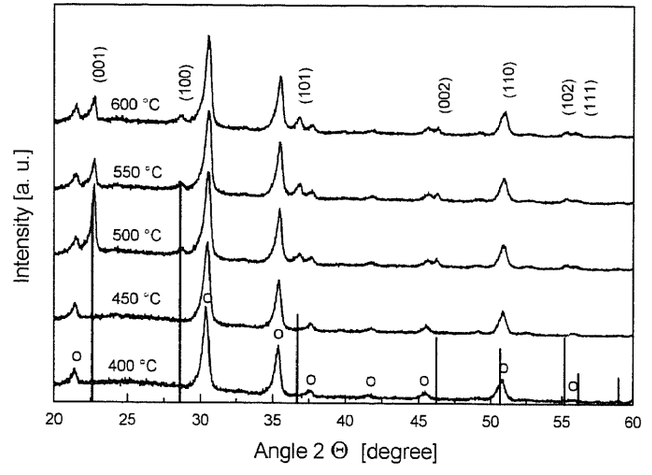

Fig. 5. X-ray diffraction of a two layers undoped Nb_2O_5 coatings (thickness approx. 120 nm) deposited on ITO coated glass sintered between 400°C and 600°C. (o: ITO-peaks. Vertical lines JCPDS 28-317 data (hexagonal structure of Nb_2O_5)) [29,33].

building up of an inorganic amorphous network, a result confirmed by X-ray diffraction (Fig. 5).

The second large exothermic double peak occurs at about 470°C and is accompanied by a smaller mass loss of 2.5%. MS analysis (Figs. 3 and 4) indicates that the loss corresponds essentially to the evolution of HCl (mass 36 and 37) and to the same fractions of organic molecules as above. The DTA peaks correspond to the crystallization process (Fig. 5). More detailed analysis indicates that in the temperature range

460–600°C the niobium oxide film exhibits the hexagonal structure (TT phase) with crystallite size of about 70 nm. The layers were found to be highly (0 0 1) oriented.

The results of electrochemical–optical studies can be classified in three groups depending on the sintering temperature. Typical results are given in Fig. 6 for amorphous coatings sintered at 450°C and for crystalline samples sintered at 500°C (low crystallinity) and 600°C (high crystallinity). All coatings are approx. 120 nm thick with a 6.6 cm^2 area. The measurements have been done using a 3-electrode optical cell containing a 1 M-solution of $LiClO_4$ dissolved in propylene carbonate as electrolyte and a $Ag/AgClO_4$ (0.01 M-solution dissolved in the used electrolyte) as reference electrode. Fig. 6 shows the cyclic voltammetry curves measured at a 50 mV/s rate between + 1 and − 2.2 V vs. $Ag/AgClO_4$ during the 50th cycle. For all materials, the reduction of Nb^V to Nb^{IV} occurs below − 1 V and the peak maximum which lies below − 2.2 V is not observed. The maximum of the oxidation peak lies at about − 1.2 V for the amorphous phase and is shifted to more negative potentials as the crystallinity increases. The width of the oxidation peak is larger for amorphous coatings indicating slower bleaching kinetics than for crystalline samples. For the crystalline samples the height of the peak increases and shifts to higher potentials with increasing temperature.

Fig. 7 shows chronoamperometric curves measured during the 50th cycle for the same samples with voltage of − 2.2 and + 1 V applied during 120 s. Coloration kinetics is always found slower than the bleaching one. For the crystalline samples kinetics of both coloration and bleaching becomes faster as the sintering temperature increases and reaches practically the same value at 600°C as those of the amorphous phase at 450°C. It is noted, especially for the layers sintered at 500°C and 550°C, that the time necessary to obtain either a full coloration or full bleaching is longer than the 120 s used in the experiments. The diffusion coefficients D for Li as determined by

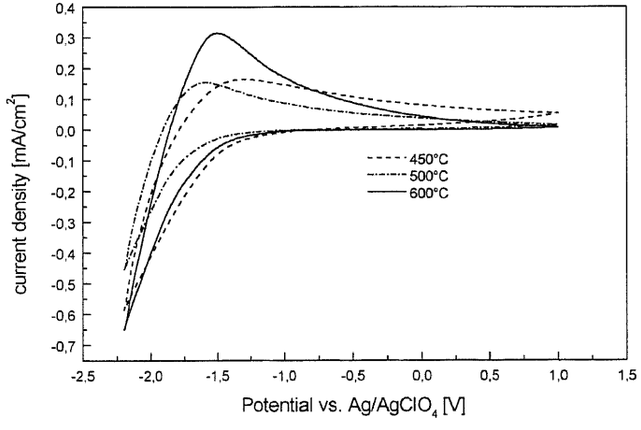

Fig. 6. 50th cycle voltammetry curves of two layers Nb_2O_5 coatings (thickness approx. 120 nm) sintered at 450°C (amorphous) and 500°C and 600°C (crystalline) [29,33].

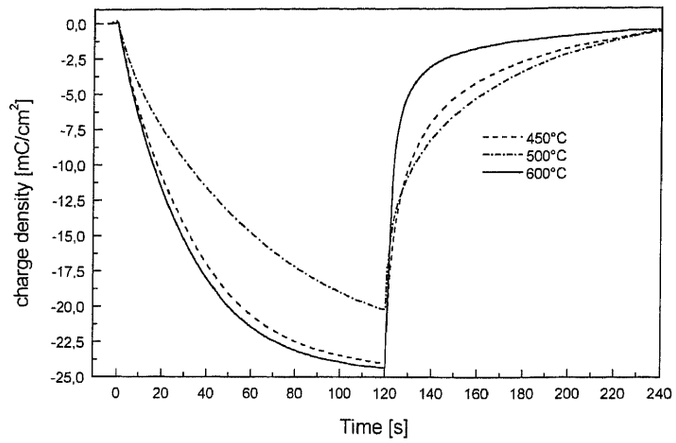

Fig. 7. 50th chronoamperometric cycle (− 2.2 ; + 1.0 V vs. $Ag/AgClO_4$) of two layers Nb_2O_5 coatings (thickness approx. 120 nm) sintered at 450°C (amorphous) and 500°C and 600°C (crystalline) [29,33].

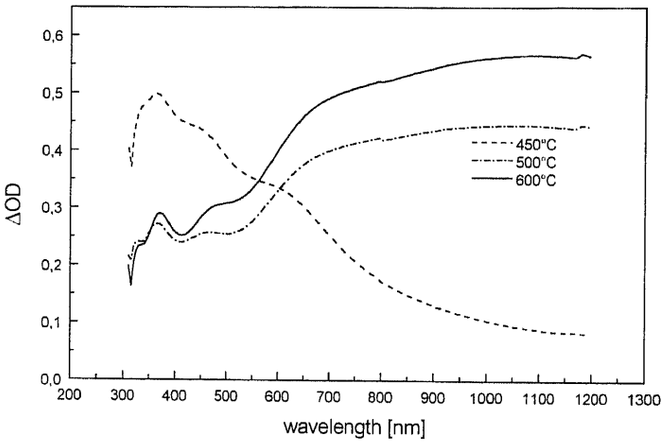

Fig. 8. Spectrum of the optical density change ΔOD of two layers Nb_2O_5 coatings (thickness approx. 120 nm) sintered at 450°C (amorphous) and 500°C and 600°C (crystalline) measured during the 50th chronoamperometric cycle (− 2.2 V,120 s; + 1.0 V,120 s vs. $Ag/AgClO_4$) [29,33].

analyzing the time behavior $I(t) \sim D^{0.5} t^{-0.5}$ [34] are in the range of 10^{-11} cm²/s and slightly increase with the sintering temperature.

Fig. 8 shows the spectral dependence of the change of the optical density ($\Delta OD = -\log_{10}(T_{bleached}/T_{colored})$ of the same samples measured during the 50th chronoamperometric cycle. The spectra are quite different and reflect the fact that the coatings, when seen in transmission, color brown in the amorphous state ($T < 450$°C) and blue in the crystalline state (TT phase for $T > 500$°C). For both the types of

morphology ΔOD increases with the sintering temperature reflecting faster kinetics as discussed above (Fig. 7)

To make practical devices, it is mandatory to know the electrochemical and optical behavior as a function of the number of applied electrochemical cycles. The optical change and amount of Li^+ charge inserted and extracted have been measured up to 5000 chronoamperometry or voltammetry cycles under the above specifications. Strong variations have been found for the amorphous coatings where ΔOD strongly increases up to the 50th cycle. This observation however only reflects the fact that the coloration and bleaching kinetics became faster with the number of cycles and that the time scale used to apply the potentials (120 s) were not long enough to obtain data for a reasonable comparison. It is, nevertheless, practically safe to say that the layers exhibit stable optical and electrochemical properties up to at least 5000 cycles with a coloration efficiency of 18.8 cm²/C at 550 nm (amorphous coatings) and that the coloration kinetics becomes slower and bleaching kinetics faster as the number of cycles increases. Similar responses, but not as strongly marked, were also found with the low crystalline coatings sintered at 500°C. The layers are also stable up to at least 5000 cycles but the coloration efficiency at 550 nm is lower, approx. 15.3 cm²/C. Similar results with 18 cm²/C have been reported by Macek et al. [31]. The layers sintered at 600°C behave similarly to those sintered at 500°C. However, coloration kinetics slows significantly with increasing number of cycles but the coloration efficiency remains constant at approx. 16.4 cm²/C. This value is slightly higher than that determined for films sintered at 500°C but somewhat smaller than the 21.9 cm²/C (measured at 600 nm) reported previously for films obtained from Nb chlorobutoxide [26,28] and the 35 cm²/C obtained for films made with Nb ethoxide but measured under H^+ insertion at 700 nm [19]. The values are, nevertheless, significantly lower than those reported for sol–gel WO_3 layers, the best EC coatings at present, which possess a coloration efficiency of about 50 cm²/C after sintering at 220°C [35]. It is also worth mentioning the value of 35 cm²/C obtained by Yoshimura et al. for Li^+ insertion into a niobia film made by DC magnetron sputtering [11] and the very high coloration efficiency of 160 cm²/C measured at 550 nm in the early stages of coloration by H^+ insertion by Maruyama et al. [10] for an amorphous niobia film made by a CVD process.

All these results indicate that *sol–gel* made niobium oxide is an interesting candidate to realize solid-state EC cells as it results in good coating, offers the possibility to get thick transparent coatings and shows reasonable coloration efficiency and high reversibility and stability under H^+ or Li^+ insertion. However, the results have been quite disappointing till today. Avellaneda [36] realized a cell with the configuration glass/ITO/Nb_2O_5/electrolyte/CeO_2–TiO_2/ITO/glass. By switching between + 1.5 and − 2.0 V only a very small Li insertion has been observed, typically 2.5 mC/cm² but no coloration has been observed. Schmitt [33] using the same configuration with a 125 nm thick Nb_2O_5 and a 240 nm thick CeO_2–TiO_2 counter-electrode also measured a very small Li insertion (<0.25 mC/cm² after switching between − 2.5 and + 1 V during 120 s) with a corresponding change in optical density at 500 nm lower than 0.01! Only Orel et al. [30,31,37] succeeded to observe a transmission change between 60% and 33% with a sol-gel SnO_2:Sb(7%):Mo (10% layer as

counter-electrode (IS) switching between -4.0 V(!) and $+2.0$ V during 120 s. Due to the very high negative applied potential, the cell had a very poor stability of < 500 cycles. These results have been explained by Schmitt et al. [33,38] using a model originally developed by Bullock and Branz [39] as being due to the too large difference existing between the internal (Fermi) potential of pure Nb_2O_5 and the ion-storage electrodes (see also below).

2.2. Doped niobium oxide sol–gel coatings and devices

Niob(V)oxide has been also used as a doping material for already known electrochromic materials. Amarilla et al. [40] for instance have prepared $NbVO_5$ bronze powder from solutions of vanadyl tri-tert-butoxide and $NbCl_5$ in isopropyl alcohol. Li^+ insertion and extraction was verified and the powders changed their color from yellow to dark gray on reduction. On the other side, Niob(V)oxide has also been doped with different compounds. Machida et al. [41] have obtained EC layers by co-sputtering niobium oxide with SnO_2 and Li_2O in order to increase the ionic conductivity of the layer. They observed much faster bleaching kinetics with the nominal composition $40Li_2O \cdot 35WO_3 \cdot 25Nb_2O_5$ compared to unlithiated films. Özer et al. [42] also tried to increase the ionic conductivity of sol–gel niobium oxide by incorporating lithium ethoxide into the sol. Films made by the spin coating technique by these authors had a conductivity as high as 8×10^{-7} S/cm but the increase in the EC coloration was only slight. In order to increase bleaching kinetics as reported in Ref. [41], Orel et al. [30,31] incorporated $LiCF_3SO_3$ into $NbCl_5$/propanol/acetic acid sols. A much better reversibility for Li^+ ions was observed and the crystalline layers made with a molar ratio $Li/Nb = 0.1$ were found to color gray when seen in transmission after sintering at 500°C. Quite high transmission changes, down to $T = 10\%$, have been obtained in the whole UV-visible range and all-solid-state EC cells have been realized [37] (see below). Following a report indicating that the morphology and surface structure of sol–gel TiO_2 was beneficial for Li^+ insertion, Avellaneda et al. [43] prepared mixed $(Nb_2O_5)_x - (TiO_2)_{1-x}$ $(0 < x < 1)$ layers, by adding titanium isopropoxide to $NbCl_5$/isopropanol/acetic acid sols. Homogeneous, crack-free coatings have been obtained up to 600°C and it was possible to insert Li^+ for all x values. A blue color under Li insertion was already observed in 400°C sintered films. An increase of the charge exchanged was observed as a function of the number of cycles.

The most detailed development has been made recently by Schmitt et al. who mixed $NbCl_5$/ethanol/acetic acid sols with compounds of Li (incorporated as $LiCF_3SO_3$ or lithium acetate), Ti (as $[(CH_3)_2CHO]_4Ti$), Sn (as $SnCl_4 \cdot 5H_2O$), Zr (as $ZrOCl_2 \cdot 8H_2O$) and Mo (as $H_3Mo_{12}O_{40}P \cdot xH_2O$) to study the influence of the doping on the EC properties of sol–gel coatings sintered between 400°C and 600°C [29,33] and devices [33,38]. The overall behavior of the DTA/TG curves was found similar to that shown in Fig. 2. However, depending on the type and amount of doping, the temperature of the formation of the inorganic amorphous network and of the crystallization processes were slightly different. Except for Mo doping all layers were found amorphous between approx. 250°C and 450°C and after Li^+ insertion the color in transmission

were brown as for the pure niobium oxide. However, besides the already known TT and T phases leading to a blue coloring effect, other structural phases such as $LiNb_3O_8$, $Ti_2Nb_{10}O_{29}$, Nb_2O_{29}, etc., have been observed at higher sintering temperature. In their presence the layers colored gray under Li^+ insertion. A detailed analysis of these results shows that the color of the layers is essentially dependent on the size of the crystallites and not on the crystal structure of the materials.

The three typical spectra observed in this study are shown in Fig. 9. A shift of the peak maximum of the spectra as a function of the morphology was also observed for WO_3. Amorphous layers have an absorption maximum at 900 nm while for well crystalline layers the peak lies at 1400 nm [44,45]. However, as both peak maxima are lying in the infrared, the resulting color of both the coatings remain blue. The absorption mechanism for the brown amorphous niobia layer is thought to arise from polaron absorption. As the crystalline order increases the absorption band becomes broader and the blue color can probably be explained by the Drude model in which the absorption is essentially governed by interaction with free electrons (high reflection). However, opposite conclusions were obtained by Orel et al. [46].

Layers sintered between 450°C and 600°C have been investigated up to 5000 cycles and, whatever the type and amount of doping and the sintering temperature, the EC properties have been found stable. The niobium oxide layers doped with Sn and Zr are still electrochromic but no improvement has been observed, as the amount of Li^+ ions which can be inserted into the layer and consequently the change of the optical density decreased with increasing doping level. Nevertheless, the coloration efficiency remains about the same at approx. 17 cm^2/C. As it was already observed [30], the incorporation of Li^+ improves the kinetics and the coloration efficiency increased to approx. 23 cm^2/C up to a molar ratio $Li/Nb = 0.1$ for the crystalline layers sintered between 500°C and 600°C. At 450°C all the layers were amorphous and colored brown. At

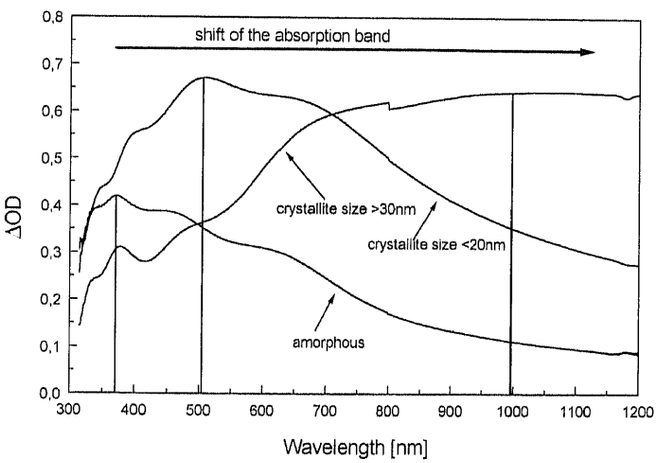

Fig. 9. Typical optical spectra (ΔOD vs. λ) of pure and Ti doped niobia EC layers after Li^+ ions insertion. Well ordered layers with crystallite size > 30 nm show a blue color, weakly ordered layers with crystallite size < 25 nm show a gray color while all amorphous layer have a brown color [29,33].

500°C only gray and brown colors have been found depending on the amount of doping while at 600°C the colors were gray and blue. With Ti doping the coloration efficiency was also found to increase for crystalline layers (up to 27 cm^2/C at 600°C). Amorphous layers coloring brown were found at 450°C and up to 500°C for high doping (Ti/Nb > 0.3). At lower doping the layers colored blue for $T > 500$°C. However, gray color was found for high doping at 600°C.

The most interesting results were found for Mo doping. The pure (0 0 1) oriented hexagonal structure was already found at 450°C for doping with 5 at% and up to 500°C with 10 at% leading to a blue color. A pure weakly crystalline orthorhombic phase ($Nb_{12}O_{29}$) with small crystallites (15–20 nm) was observed in films doped with 20 and 30 at% sintered at 450°C and 500°C leading to a gray color and a mixed structure with hexagonal Nb_2O_5 and orthorhombic $Nb_{12}O_{29}$ crystallite was observed with a 20 at% Mo doping sintered at 450°C and for all doped samples sintered at 600°C. A high doping (>15 at%) drastically favors an increase of the amount of Li^+ ions charge which can be incorporated into the layers and consequently a higher optical density change is observed.

Only two groups have reported the use of doped niobia as an EC electrode. Orel et al. [31,37] have built solid-state cells with the configuration glass/FTO/$Li_xNb_2O_5$/ormolyte/SnO_2:Sb:Mo/FTO/glass. The molar ratio was Li/Nb = 0.1 and the niobia layer was sintered at 500°C. Such cells have been switched between −4 and +2 V and exhibited a gray color in the colored state and transmission change up to 45% have been observed in the early cycles. Their lifetime was however short (<500 cycles) due to the high negative potential used to obtain a coloration which is out of the range of the stability of the EC, IS and electrolyte layers. The second successful result has been obtained by Schmitt et al. [33,38] who used the configuration glass/FTO/doped niobia/electrolyte(liquid)/CeO_2–TiO_2/FTO/glass. Applying the model developed by Bullock et al. [39], they show that, for this configuration, a reasonable coloration within the safe voltage range of ±2.5 V could only be obtained with Mo doped niobia. The most important parameters necessary to simulate the coloration behavior of the cell are the Fermi potentials of both layers (Fig. 10) which have been determined from coulometric titration curves by applying a current density of 5 μA/cm^2. The Fermi potential increases significantly with the sintering temperature (shown here for pure Nb_2O_5). It remains similar for Li and Ti doped materials but decreases drastically for Mo doped niobia. Within the safe voltage range (±2.5 V) required by the used electrolyte, all EC layers can incorporate a large amount of Li ions up to $x \cong 1$.The results are however quite different for the CeO_2–TiO_2 ion storage electrode and within the safe potential range only a small amount of Li up to $x \cong 0.14$ can be intercalated.

As the coloration efficiency for doped niobia is at most about 25 cm^2/C, a minimum amount of charge of approx. 40 mC is necessary to obtain a change of the optical density of about 1. According to the results discussed above this is readily realizable in an electrochemical cell with all niobia layers having a thickness of about 300 nm. In a device this charge should be switched back and forth between the EC and IS electrodes. The model simulation shows that the best EC material is Mo doped niobia and that the thickness of the CeO_2–TiO_2 IS electrode should be typically 10–20 times

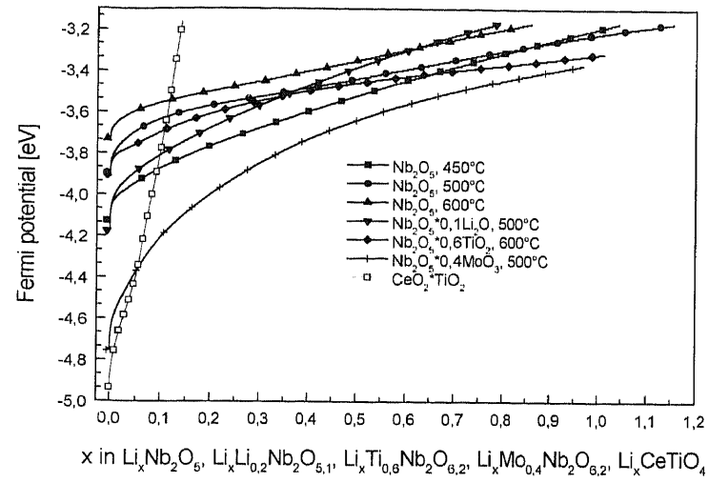

Fig. 10. Fermi potential curves determined from coulometric titration after the 50th chronoamperometric cycle for different pure and doped niobium oxides as well as for the ion storage layer TiO_2–CeO_2 [33,38].

thicker than that of the EC layer! This, of course, is technically not realizable. Cells made with smaller thickness will color but with a lower optical density variation. Fig. 11 shows the change of light transmittance, $\Delta\tau$, calculated according to DIN EN 410 (weighted with the light function D_{65} and the human eye sensibility for day light $V(\lambda)$) vs. the number of cycles of 6×8 cm^2 devices made with a 180 nm thick $Nb_2O_5 \cdot 0.4$ Mo EC electrode sintered at 600°C and a TiO_2–CeO_2 IS electrode made according to Ref. [47] with a thickness varying between 240 nm (1 layer) to approx. 950 nm (4 layers). A voltage of ±2.5 V was applied during 120 s (each cycle).

The results obtained confirm only partially the simulation results. A thicker IS layer leads effectively to an increase in the transmission change but the response does not vary linearly. This is probably due to the fact that the ionic conductivity of these layers is low (which is not taken into account by the model). In the early cycles the change of transmission is low but it strongly increases with the number of cycles, then passes by a maximum and decreases. It is believed that the deterioration of the cells is due to a corrosion effect between the electrolyte and the IS electrode. The highest amount of charge exchanged was 18 mC/cm^2 obtained with 3 IS layers and the maximum change in transmission was $\Delta\tau = 0.28$. The best cells were stable up to about 20 000 cycles. These results however clearly show that a better IS electrode having a flatter Fermi potential variation and allowing a much higher Li^+ ions capacity should be developed in order to use niobium oxide as an EC material for the realization of EC devices. With a $CeVO_4$ layer having a thickness about twice that of the Mo doped niobium oxide layer, a value of $x = 1.4$ can be reached. However, such layers are not yet stable and their capacity for Li^+ insertion becomes very low after 300 cycles [48].

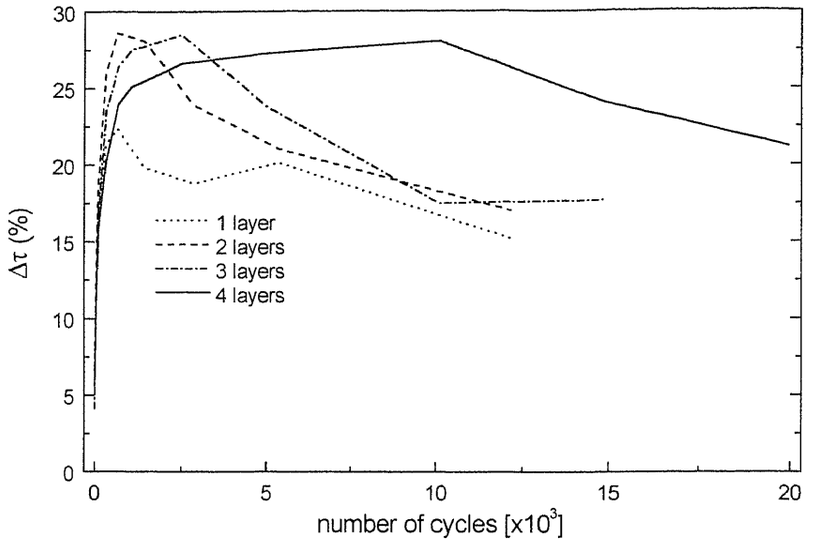

Fig. 11. Change of light transmittance $\Delta\tau$ calculated according to DIN EN 410 (weighted with the relative light function D_{65} and the human eye sensibility for day-light $V(\lambda)$) vs. the number of cycles of $6 \times 8\,cm^2$ devices made with a 180 nm thick $Nb_2O_5 \cdot 0.4$ Mo EC electrode and a TiO_2–CeO_2 IS electrode having a thickness varying between 240 nm (1 layer) to approx. 950 nm (4 layers). Applied voltage : -2.5; $+2.5$ V each during 120 s [33,38].

3. Batteries

A great interest exists on the development of secondary lithium batteries based on lithium intercalation electrodes. There is an increasing need for rechargeable microbatteries that can be fully charged in the voltage range 2–3 V as it is required by most integrated circuits. Niobium pentoxide is one of the few candidates for 2 V class rechargeable Li batteries. The material has been practically used as a negative electrode in $Li_xNb_2O_5/V_2O_5$ [49] and more recently in $LiAl/Li_xNb_2O_5$ secondary batteries. The electrodes are usually made by compacting a mixture of Nb_2O_5 powder prepared by heat treatment of niobium hydroxide between 600°C and 1000°C and graphite as conductive filler in the form of 0.5 mm thick pellets. A recent report on the properties of such pellets having the hexagonal, orthorhombic and monoclinic modification of niobia is given by Kumagai et al. [50]. Although the sol–gel process appears to be an interesting way to prepare thick films and powders for such applications, no reports are available. Guo and the author [51] have prepared thick sol–gel pure niobium oxide films (TT phase) using a process reported in Ref. [52] and determined the intercalation of Li^+ ions by measuring titration curves in a $LiClO_4$/propylene carbonate electrolyte under a current density of $0.1\,mA/cm^2$. The second discharge–charge curves is shown in Fig. 12. The layer displays a high discharge capacity, up to 220 mAh/(g-oxide) with charge–discharge cycling between 1.5 and 3 V vs.

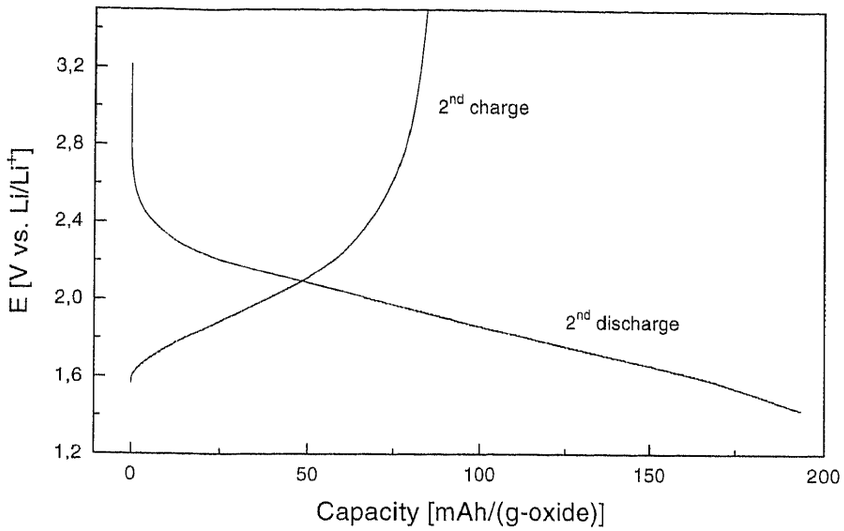

Fig. 12. Second cycle discharge–charge curves of a 6 μm thick Nb_2O_5 coating sintered at 520°C. Current density $0.1\,mA/cm^2$ [51].

Li/Li^+. The electrochemical reaction leads to the formation of $Li_xNb_2O_5$ with a maximum of $x = 3$ (see also Fig. 12 where 100 mAh/(g-oxide) corresponds to $x = 1$). For higher x values, the discharge curve reaches a lower plateau, indicating probably the formation of a ternary phase. Fig. 10 shows similar curves taken for other niobium oxide compounds (to convert the data to the units of Fig. 12, the ordinate of Fig. 10 should be recalculated as E (V vs. Li/Li^+) $= -(E_{fermi} + 1.455)$ and the abscissa as capacity (mAh/(g-oxide) $= 100x$). Although the measurements have been realized with thinner films and not extended to higher values of x, the figure shows that the capacity of all doped layers was as high as 100 mAh/(g-oxide) and that the voltage range could be adjusted easily by the choice of the doping. In this sense Ti doping looks attractive for 2 V batteries as the slope of the discharge is flatter and Mo doping seems suitable for 3 V batteries. Compared to the results shown in Ref. [50], the sol–gel process shows that it might be possible to make thinner batteries using a dip or spin coating process, followed by a sintering at temperature as low as 520°C, the charge capacity of the films could be 1.4 times higher and the stability of the discharge–charge cycles could be probably higher as all layers were found stable at least up to 5000 EC cycles.

4. Solar cells

Since the discovery by Graetzel [53,54] that a dye sensitization of a porous coating of crystalline TiO_2 nanoparticles could be used for the development of solar cells, many other wide-band-gap semiconductors, including niobia, have been studied.

Most of the cells tested till now consist of a porous coating of crystalline nanoparticles on a transparent conducting glass substrate whose crystalline nanoparticles with a chemically adsorbed monolayer of a Ru(II)-complex. The system can be completed by an electrolyte with an iodide/triiodide redox mediator and a counter-electrode comprising a catalyst. For TiO_2 the overall conversion efficiency measured under 1000 W/m^2 solar simulator irradiation varies typically between 7% and 12% with an open-circuit photovoltage of 0.7–0.8 V. As the conversion efficiency strongly depends on the surface area available to sensitize the semiconducting particles, the sol–gel process is therefore particularly adequate for the preparation of such porous coatings.

Several works have been reported with niobia coatings made by the *sol–gel* process. Preliminary photoelectrochemical studies have shown that pure sol–gel niobia coatings (without dye sensitization) exhibited a photoelectric effect in the UV region, however, somewhat smaller than that of TiO_2 films [55,56]. Thin films ($\sim$100 nm) were deposited by spin coating using sols prepared by dissolving $NbCl_5$ in n-butyl alcohol and cyclohexane (chloroalkoxide method). The films appear as an agglomeration of approx. 300 nm size grains made themselves from crystalline particles smaller than 100 nm. Hu et al. [57] prepared niobia colloidal suspensions by hydrolyzing niobium alkoxide solutions ($Nb(OEt)_5$ dissolved in ethanol added to a triethylamine ethanolic aqueous solution and water and autoclaving at 250°C. The films fired at 500°C had the TT structure, were porous and presented a different morphology consisting of needles. The authors only mention that a cell made with such a layer after coating with a Ru(II)-complex gave a current conversion efficiency (IPCE) of 40% and an open-circuit voltage of 0.4 V, both values being much smaller than those obtained with TiO_2. Wolf [58], using similar preparation techniques, showed that the specific BET area of the sintered materials was in the range of 30–50 m^2/g and that the coatings had an IPCE of 33% at 550 nm. The cells of size 0.45 cm^2 presented an almost constant conversion efficiency of 2.5% under simulated solar light irradiation up to 100 mW/cm^2 (1 sun). The open-circuit voltage, short-circuit current and IPCE were found to decrease steadily by doping niobium oxide with Ta ($Nb_{1-x}Ta_x)_2O_5$ up to $x = 0.25$.

Sayama et al. [59] prepared 1 cm^2 dye sensitized cells where 6–8 μm thick niobia electrode was made by spreading a slurry of either commercial powders or powders made by calcining niobium hydroxide between 300°C and 900°C. The coatings were porous and appear as an agglomeration of 100–200 nm size particles. However, the overall photoelectrochemical results were not good. An improvement was obtained by dropping niobium alkoxide on 700°C sintered coatings (made from Nb hydroxide) and then calcining the system again at 500°C. The surface of the particles became rougher, quite similar to what was observed in Ref. [56] and thus allowed to increase the amount of dye adsorbed on the surface by a factor of 1.2 resulting in an increase of the photoconductivity between the particles. Nevertheless, the overall solar-to-electric conversion efficiency remained low, typically 2% under AM1.5 (100 mW/cm^2) irradiation.

Better results have been obtained in the author's group [52,59]. The sol–gel coatings were made by spin deposition of partially hydrolyzed ethanolic niobia sols submitted to an ultrasonic treatment and then boiled under reflux. Each layer was

Table 1
Structural parameters for two different niobium oxide layers [60,61] and a TiO_2 layer [62] and electric parameters of solar cells made with such layers measured under various irradiance

Electrode	BET area (m^2/g)	BJH pore size (nm)	Roughness	Irradiance (W/m^2)	U_{oc} (V)	i_{sc} (mA/cm^2)	FF	η (%)
Nb_2O_5[a] (0.2 cm^2)	25	9	200	100	0.57	1.6	0.55	4.9
				900	0.61	7.0	0.44	2.2
Nb_2O_5 + PE G + C[a] (0.2 cm^2)	44.1	9	530	100	0.64	2.11	0.60	8.1
				900	0.67	6.94	0.62	3.0
TiO_2[b] (0.4 cm^2)	104	20	780	1000	0.83	11.3	0.71	6.7

[a]From Refs. [60,61].
[b]From Ref. [62].

dried after deposition at 400°C and then the finally obtained 5–8 μm thick coatings were sintered between 400°C and 650°C. The BET surface area of the material was found to increase with sintering temperature up to 25 m^2/g after sintering between 500°C and 550°C and then to strongly decreases down to 13 m^2/g at 650°C while the BJH average pore size diameter was steadily increasing from 8.0 up to 23.7 nm. The amount of dye which could be adsorbed on a 10 μm thick layer was 3.3 mol/cm^2 corresponding to a roughness factor of 200, assuming that each dye molecule occupies an area of 1 nm^2. The values of the electrical parameter of 0.2 cm^2 solar cell sintered at 520°C and sensitized with the Ru(II)-complex are shown in Table 1 for two different solar intensity illumination.

Up to about 0.1 sun (10 mW/cm^2) irradiation the solar-to-electric conversion was 4.9% and steadily decreased with increasing light intensity down to a value of 2.2% for 1 sun. The low efficiency was thought to arise from too low BET surface area and too small pore diameter of the niobia coatings in comparison of TiO_2 coatings (53 m^2/g and 16 nm, respectively). A modification of the morphology of the films was obtained by adding to the sol a polymeric ligand and carbon soot [61]. The nanoscopically phase-separated film should allow to obtain higher values of the parameters as extra micropores should be produced during the burn-out of the organic products. Although the average porosity (about 45%) and the BJH pore size diameter (9 nm) did not change, the BET surface area, the amount of dye adsorbed and the roughness factor were all effectively increased to about 45 m^2/g, 8.8 mol/cm^2 and 530, respectively. For a cell of the same size (0.2 cm^2), the solar-to-electric conversion efficiency was increased from 4.9% to 8.1% under 0.1 sun irradiation, but still was found to diminish with the increase of the light intensity down to about 3.0% at 1 sun (Table 1). The current density vs. voltage is shown for both types of niobia electrodes for a 0.2 cm^2 cell in Fig. 13 and the variation of the solar-to-electric conversion efficiency η with the solar light intensity for Nb_2O and TiO_2 [63] is shown in Fig. 14.

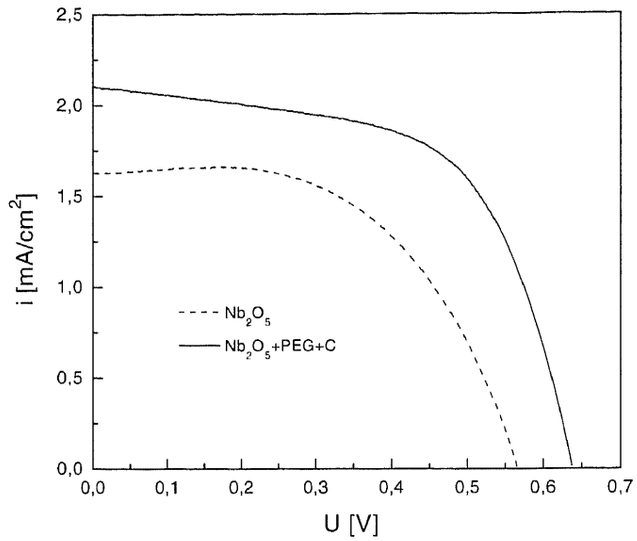

Fig. 13. Photocurrent–voltage characteristics of 0.2 cm² solar cells made with Ru(II)-complex sensitized sol–gel niobia films measured under 10 mW/cm² solar irradiation (0.1 sun) [60,61].

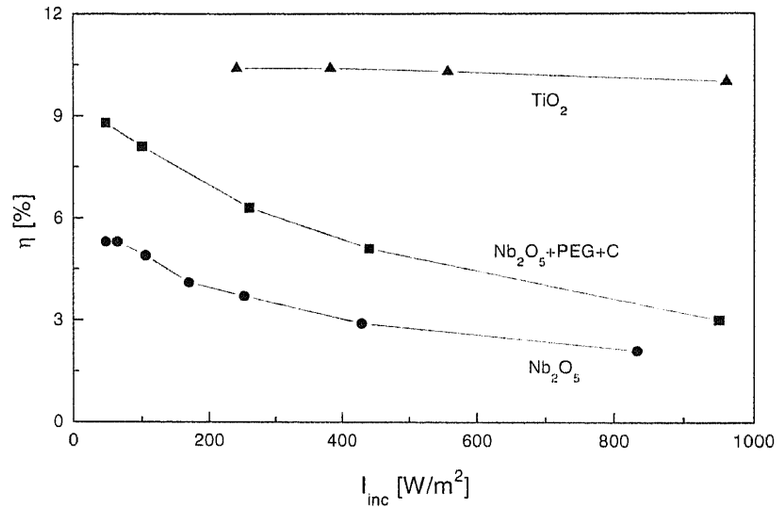

Fig. 14. Solar-to-electric conversion efficiency of 0.2 cm² solar cells made with niobia electrodes [60,61] and a 0.4 cm² TiO_2 cell [63].

The results obtained with sensitized niobia electrodes are quite promising and practically equal to those obtained for TiO_2 electrode at low illumination level. The morphology of the layers, especially the average size and shape of the pores, seems to be the most important factor that has to be improved.

5. Catalysis

The preparation of catalytic supports is also an important task today. The sol–gel processing is surely a quite promising process to achieve this goal. Niobia is known as an important constituent in heterogeneous catalysts, acting either as an active catalytic component or as an agent in multicomponent formulations. Several papers have been published on the catalytic properties of niobia, but the materials were rarely prepared by a sol–gel process but essentially by calcining niobic acid ($Nb_2O_5 \cdot nH_2O$) at high temperature or by the incipient-wetness impregnation method using, for example, niobium oxalate or ethoxide solution with various supports [64] (see for instance the special edition of Refs. [65,66]). When niobic acid is heated to eliminate the residual water, which is completed at about 300°C, and to create strong acidic centers observed already at $T > 100$°C, its surface area and the amount of catalytic OH groups on the surfaces are continuously reduced as the temperature increases. These transformations and the loss of porosity are irreversible and the material becomes practically inactive at about 500°C when niobia starts to crystallize. The crystallization of niobia could be inhibited while keeping a very high surface area by drying niobia wet xerogels under CO_2 supercritical conditions at 85 kbar and 240°C (formation of aerogels). Rabêlo et al. [67,68] compared the catalytic behavior of niobia aerogels, xerogels and commercial products (CBMM) sintered between 300°C and 700°C for the cracking reaction of n-heptane. The sols have been prepared using the Na route [25], similar to that used for the preparation of EC films mentioned above. After a 12 h calcination at 300°C the BET surface area of aerogels was 328 m^2/g, a factor 2.4 times higher than that of the commercial product. The value lowers to 180 m^2/g for a calcination at 500°C but the factor increases to 3.2. At higher temperatures a strong reduction of the BET area was observed (40 m^2/g). Aerogels were also found to possess less labile hydroxyls and more acidic sites than the commercial product. The catalytic reaction rate of n-heptane cracking measured at 420°C after 2 min was 2.3×10^{-3} and 5.3×10^{-4} mol $nC_7/h \cdot g$ for aerogels sintered at 300°C and 500°C, respectively, and a conversion efficiency as high as 20% was obtained for 420°C. Both results are much higher than those obtained with the commercial product.

6. Conclusion

This paper has briefly reviewed the state of the art achieved with pure or doped niobium pentoxide made by sol–gel processes. Since its first preparation in 1986, many laboratory developments have been done for the use of this material either in the form of thin or thick coatings, powders, xerogels or aerogels. Pure and doped niobium oxide coatings exhibit quite good and stable properties for the intercalation of H^+ and Li^+ ions and are promising compounds for the development of electrochromic devices and 2–3 V mini batteries. 100–300 nm thick layers can be used reversibly either as EC or IS electrodes with a lifetime higher than 10^4 cycles. Depending of the type of doping and the sintering temperature the color of the layers

seen in transmission may be brown, gray or blue. Their use in such devices is however dependent on the discovery of an adequate counter-electrode. High amount of Li^+ ions can be charged and discharged in thick Nb_2O_5 coatings (several μm) with a capacity up to 220 mAh/(g-oxide) in the potential range 1.5–3 V. Such layers can be used for the development of mini batteries. As niobium oxide has quite similar semiconducting properties as TiO_2 its use in the form of thick porous coatings for the development of nanocrystalline solar cells has also been demonstrated. The 9% solar-to-electric conversion obtained at low light intensity illumination, $< 100\,W/m^2$, is comparable to that obtained with titania. Such coatings are therefore quite promising but a development is still needed to improve the morphology of the layers in order to increase the efficiency at high illumination level. Although the sol–gel process is an adequate method to obtain highly porous materials, a necessary condition in catalysis, very few works have been done in this interesting field. Nevertheless, niobia aerogels have been shown to exhibit better properties than commercial products for the cracking reaction of n-heptane.

Acknowledgements

The author thanks the Federal Ministry for Education, Research and Technology of Germany and the State of Saarland (Germany) for their financial support.

References

[1] Gmelins Handbuch der Anorganischen Chemie, Niob und Sauerstoff B1 (1970) 49; Verlag Chemie GmbH, Weinheim/Bergstrasse.
[2] J. Eckert, Niobium and niobium compounds, in: B. Elvers, S. Hawkins, G. Schulz, eds., Ullman's Encyclopedia of Industrial Chemistry, 5th Edition, Vol. A17, 1990, pp. 251–264.
[3] G. Brauer, Zeitschrift für anorganische und allgemeine Chemie 248 (1) (1941) 1.
[4] H. Schäfer, R. Gruehn, F. Schulte, Angew. Chem. 78 (1) (1966) 28.
[5] E.I. Ko, J.G. Weissman, Cataly. Today 8 (1990) 27.
[6] C. Alquier, M.T. Vandenborre, M. Henry, J. Non-Cryst Solids 79 (1986) 383.
[7] P. Griesmar, G. Papin, C. Sanchez, J. Livage, Chem. Mater. 3 (1991) 335.
[8] B. Reichman, A.J. Bard, J. Electrochem. Soc. 127 (1980) 241.
[9] B. Reichman, A.J. Bard, J. Electrochem. Soc. 128 (1981) 344.
[10] T. Maruyama, T. Kanagawa, J. Electrochem. Soc. 141 (1994) 2868.
[11] K. Yoshimura, T. Miki, S. Iwama, S. Tanemura, Jpn. J. Appl. Phys. 34 (1995) L1293.
[12] G.R. Lee, J.A. Crayston, J. Mater. Chem 6 (1996) 187.
[13] A. Agrawal, J.P. Cronin, R. Zhang, Solar Energy Solar Cells 31 (1993) 9.
[14] M.A. Aegerter, Proceedings of the International Congress on Glass, Vol. 1, Beijing, 1995, pp. 95–105.
[15] M.A. Aegerter, Sol-gel Chromogenic materials and devices, in: R. Reisfeld, C. Jorgensen (Eds.), Structure and Bonding: Optical and Electronic Phenomena in Sol-gel Glasses and Modern Applications, Vol. 85, Springer, Berlin, 1996, pp. 149–194.
[16] M.A. Aegerter, C.O. Avellaneda, A. Pawlicka, M. Atik, J. Sol–Gel Sci. Technol. 8 (1997) 689.
[17] G.R. Lee, J.A. Crayston, J. Mater. Chem. 4 (7) (1994) 1093.
[18] R.C. Faria, L.-O. de, S. Bulhoes, J. Electrochem. Soc. 141 (1994) L29.
[19] B. Ohtani, K. Iwai, S.-I. Nishimoto, T. Inui, J. Electrochem. Soc. 141 (1994) 2439.
[20] N. Özer, T. Barreto, T. Büyüklimanli, C.M. Lampert, Solar Energy Mater. Solar Cells 36 (1995) 433.

[21] N. Özer, D.-G. Chen, C.M. Lampert, Thin Solid Films 277 (1996) 162.
[22] C.O. Avellaneda, M.A. Macedo, A.O. Florentino, M.A. Aegerter, in: V. Wittwer, C.G. Granqvist, C.M. Lampert (Eds.), Optical Materials Technology for Energy Efficiency and Solar Energy Conversion XIII, SPIE, Vol. 2255, SPIE, Bellingham, Washington, USA, 1994, pp. 38–51.
[23] C.O. Avellaneda, M.A. Macedo, A.O. Florentino, D.A. Barros Filho, M.A. Aegerter, in: J.D. Mackenzie (Ed.), Sol–Gel Optics III, SPIE, Vol. 2288, SPIE, Bellingham, Washington, USA, 1994, pp. 422–434.
[24] M.A. Aegerter, C.O. Avellaneda, in: E.J.A. Pope, S. Sakka, L. Klein (Eds.), Sol–Gel Science and Technology, Ceramic Transactions, Vol. 55, The American Ceramic Society, Westerville, OH, USA, 1995, pp. 223–234.
[25] R.C. Mehrotra, J. Non-Cryst. Solids 100 (1988) 1.
[26] A. Pawlicka, M. Atik, M.A. Aegerter, J. Mater. Sci. Lett. 14 (1995) 1568.
[27] C.O. Avellaneda, A. Pawlicka, M.A. Aegerter, J. Mater. Sci. 33 (1998) 2181.
[28] M. Schmitt, S. Heusing, M.A. Aegerter, A. Pawlicka, C. Avellaneda, Solar Energy Mater. Solar Cells 54 (1998) 9.
[29] M. Schmitt, M.A. Aegerter, in: C.M. Lampert (Ed.), Switchable Materials and Flat Displays, SPIE, Vol. 3788, SPIE, Bellingham, Washington, USA, 1999, pp. 93–102.
[30] M. Macek, B. Orel, U. Opara Krasovec, J. Electrochem. Soc. 144 (1997) 3002.
[31] M. Macek, B. Orel, Solar Energy Mater. Solar Cells 54 (1998) 121.
[32] D.A. Barros Filho, P.P. Abreu Filho, U. Werner, M.A. Aegerter, J. Sol Gel Sci. Technol. 8 (1997) 735.
[33] M. Schmitt, Ph. D. Thesis, Institut für Neue Materialien, INM and Universität des Saarlandes, Saarbrücken, Germany, 2000.
[34] A.J. Bard, L.R. Faulkner, Electrochemical Methods, Fundamentals and Applications, Wiley, New York, 1980.
[35] S. Cramer v. Clausbruch, Ph. D. Thesis, Institut für Neue Materialien, INM and Universität des Saarlandes, Saarbrücken, Germany, 2000.
[36] C.O. Avellaneda, Ph. D. Thesis, University of Sao Paulo, Brazil, 1999.
[37] B. Orel, U. Opara Krasovec, M. Macek, F. Svegl, U. Lavrencic Stangar, Solar Energy Mater. Solar Cells 56 (1999) 343.
[38] M. Schmitt, M.A. Aegerter, in: C.M. Lampert (Ed.), Switchable Materials and Flat Displays, SPIE, Vol. 3788, SPIE, Bellingham, Washington, USA, 1999, pp. 75–83.
[39] N. Bullock, H.M. Branz, in: C.M. Lampert, S.K. Deb, C.G. Granqvist, eds., Optical Materials Technology for Energy Efficiency and Solar Energy Conversion XIV, SPIE, Vol. 2531, SPIE, Bellingham, Washington, USA, 1995, pp. 152–160.
[40] J.-M. Amarilla, B. Casal, J.-C. Galvan, E. Ruiz-Hitzky, Chem. Mater 4 (1992) 62.
[41] N. Machida, M. Tatsumisago, T. Minami, J. Electrochem. Soc. 133 (1986) 1963.
[42] N. Özer, C.M. Lampert, Solar Energy Mater. Solar Cells 39 (1995) 367.
[43] C.O. Avellaneda, A. Pawlicka, M. Atik, M.A. Aegerter, Proceedings of XVII International Congress on Glass, Vol. 4, Chinese Ceramic Society, Beijing, 1995, p. 465.
[44] O.F. Schirmer, V. Wittwer, G. Brandt, J. Electrochem. Soc. 124 (1977) 749.
[45] V. Wittwer, O.F. Schirmer, P. Schlotter, Solid State Commun. 25 (1978) 977.
[46] B. Orel, M. Macek, J. Grdadolnik, A. Meden, J. Solid Sate Electrochem. 2 (1998) 221.
[47] B. Munro, P. Conrad, S. Krämer, H. Schmidt, P. Zapp, Solar Energy Mater. Solar Cells 54 (1998) 131.
[48] U.O. Krasovec, B. Orel, A. Surca, N. Bukovec, R. Reisfeld, Solid State Ionics 118 (1999) 195.
[49] N. Kumagai, K. Tanno, T. Nakajima, N. Watanabe, Electrochim. Acta 28 (1983) 17.
[50] N. Kumagai, S. Komaba, N. Kumagai, Proc. MRS 575 (2000) 39.
[51] Y. Guo, M.A. Aegerter, private communication.
[52] Y. Guo, S. Heusing, M.A. Aegerter, Adv. Sci. Technol. (Faenza, Italy) 24 (1999) 585.
[53] B. O'Reagan, M. Graetzel, Nature 343 (1991) 737.
[54] M. Graetzel, MRS Bull. XVIII (1993) 61.
[55] D.A. Barros, P. Filho, P. Abreu Filho, U. Werner, M.A. Aegerter, J. Sol–Gel Sci. Technol. 8 (1997) 735.
[56] D. de, A. Barros Filho, D.W. Franco, P.P.A. Filho, O.L. Alves, J. Mater. Sci. 33 (1998) 2607.
[57] L. Hu, M. Wolf, M. Graetzel, Z. Jiang, J. Sol–Gel Sci. Technol. 5 (1995) 219.

[58] M. Wolf, Ph. D.Thesis, Ecole Polytechnique Fédérale de Lausanne, Switzerland, 1998.
[59] K. Sayama, H. Sugihara, H. Arakawa, Chem. Mater. 10 (1998) 3825.
[60] Y.P. Guo, M.A. Aegerter, Thin Solid Films 351 (1999) 290.
[61] Y.P. Guo, M.A. Aegerter, Proceedings of EUROMAT 1999, K. Grassie, E. Teuckhoff, G. Wegner, J. Hausselt, H. Hanselka, eds., München, Germany, September 27–30, to appear.
[62] A. Kay, M. Graetzel, Sol. Energy Mater. Sol. Cells 44 (1996) 99.
[63] M.K. Nazeeruddin, A. Kay, I. Rodicio, R. Humphry-Baker, E. Müller, P. Liska, N. Vlachopoulos, M. Graetzel, J. Am. Chem. Soc. 115 (1993) 6382.
[64] K. Tanabe, S. Okazaki, Appl. Catal. A 133 (2) (1995) 191.
[65] Catal. Today 8 (1990) 1–132.
[66] Catal. Today 57 (2000) 167–357.
[67] A.A. Rabêlo, M. Sc. Thesis, University of Sao Paulo, Brazil, 1996.
[68] A.A. Rabêlo, A. de Oliveira Florentino, D.A.G. Aranda, M. Schmal, M.A. Aegerter, Sol–Gel Processing of Advanced Materials, Ceramic Transactions, Vol. 81, The American Ceramics Society, 1998, pp. 331–336.

ELSEVIER

Solar Energy Materials & Solar Cells 68 (2001) 423–425

Solar Energy Materials & Solar Cells

www.elsevier.com/locate/solmat

Author index to volume 68

Elsevier Science B.V.